


ORIGINAL INNOVATION

Open Access



Machine learning for prediction of wind effects on behavior of a historic truss bridge

Jun Wang^{1*} , Yail J. Kim² and Lexi Kimes³

*Correspondence:
jun.wang@ucdenver.edu

¹ Corresponding author,
Post-Doctoral Fellow,
Department of Civil Engineering,
University of Colorado Denver,
Denver, CO, USA

² Professor, Department
of Civil Engineering, University
of Colorado Denver, Denver,
CO, USA

³ Structural Engineer, HDR, Inc.,
Denver, CO, USA

Abstract

This paper presents the behavior of a 102-year-old truss bridge under wind loading. To examine the wind-related responses of the historical bridge, state-of-the-art and traditional modeling methodologies are employed: a machine learning approach called random forest and three-dimensional finite element analysis. Upon training and validating these modeling methods using experimental data collected from the field, member-level forces and stresses are predicted in tandem with wind speeds inferred by Weibull distributions. The intensities of the in-situ wind are dominated by the location of sampling, and the degree of partial fixities at the supports of the truss system is found to be insignificant. Compared with quadrantal pressure distributions, uniform pressure distributions better represent the characteristics of wind-induced loadings. The magnitude of stress in the truss members is enveloped by the stress range in line with the occurrence probabilities of the characterized wind speed between 40% and 60%. The uneven wind distributions cause asymmetric displacements at the supports.

Keywords: Modeling, Machine learning, Random forest, Truss bridge, Wind

1 Introduction

Truss bridges are commonplace in civil infrastructure because of noticeable advantages, including convenient construction, economy, and familiarity. However, contemplating the light weight of truss systems, their performance may be controlled by wind load. The minimum requirements of wind load for bridge design have evolved over the last decades. A base wind speed of 44.7 m/s or 160 km/h is frequently adopted in the community and practitioners also refer to refined speeds at certain regions as per a published standard. The ASCE 7 Standard is considered one of the most comprehensive resources encompassing wind-related information (ASCE 2016). From a historical perspective, technical contents that originated from the ANSI A58.1 guideline of the American National Standards Institute (ANSI 1982) were transferred to the American Society of Civil Engineers (ASCE) in 1990 and revised to be part of an early version of ASCE 7 (ASCE 1990). Since then, several changes were made with wind speeds, factors, and other details. In 2010, ASCE 7 accommodated the principle of performance-based engineering (ASCE 2010). Contrary to previous versions built upon uniform wind hazards, a wind map was provided in compliance with

the probability of failure; specifically, Risk Categories I to IV were defined at return periods of 300 to 1700 years (ASCE 2010), which were updated with 3000 years for Category IV in 2016 (ASCE 2016). On the design of bridge structures, the American Association of State Highway and Transportation Officials (AASHTO) Load and Resistance Factor Design (LRFD) Bridge Design Specifications (BDS) embraced the wind map of ASCE 7 alongside the fastest-mile wind speed (AASHTO 2017); thereafter, a three-second gust wind speed was implemented. The fastest-mile wind speed indicates the shortest time of passing a point by a-mile-long wind (Wassef and Ragget 2014), while the three-second gust wind speed means the peak speed measured for an hour with a three-second gust duration (Lombardo 2021).

Instead of costly wind tunnel tests, numerical simulations are conducted on many occasions (Zhang et al. 2021). The concept of computational fluid dynamics is prevalent in the area of finite element modeling to examine the effects of wind load on the behavior of highway bridges (Han et al. 2018). The advancement of information technology has brought the era of new predictive modeling methodology, which is known as machine learning. The application of machine learning is enormously broad from agriculture to astronomic physics (Meher and Panda 2021; Meshram et al. 2021), and a recent state-of-the-art review articulates how this emerging technology is used for structural engineering (Thai 2022). Machine learning is classified into supervised, semi-supervised, and unsupervised groups, depending upon the type of supplied data for input and output (Wu and Snaiki 2022). Among many, reduced-order machine learning receives attention owing to its simplified formulation, rapidity, and reliability (Chen et al. 2021), and random forest is a representative branch established on the ensemble classification of multiple decision trees (Sun and Zhou 2018; Karpatne et al. 2023). In the context of accuracy control, predefined classifiers are processed and the agreement is adjusted between classified and unclassified labels (Fawagreh et al. 2014). As is the case for machine learning, the potential of random forest is remarkable in numerous disciplines (e.g., biology, bioinformatics, medicine, neuroscience, and natural disaster assessments, Boulesteix et al. 2012; Terranova et al. 2021; Zhu and Zhang 2021).

A plethora of endeavors were expended to apply random forest to solve assorted structural engineering problems. Eidetic interpretations, accuracy, and stable solutions are the benefits of this modeling approach (Li et al. 2021a). Pham et al. (2020) predicted the ultimate load of piles with a variety of input parameters (e.g., the length and diameter of piles and ground elevations). A random forest model was developed and trained using more than 2000 test data. The inferred ultimate loads showed better agreement to measured values in comparison with those of empirical equations. Li et al. (2021b) utilized a random forest algorithm for the examination of building responses under wind loading. Predicted data assisted in comprehending the complex response of the building structure. Mohammed and Ismail (2021) calculated the shear strength of concrete beams with the aid of random forest. A total of 349 specimens were employed to train the machine learning model. The coefficients of determination between the predicted and observed data were reasonably satisfactory at $R^2=0.674$ to 0.949. Notwithstanding these promising outcomes, the majority of existing evaluations were concerned with laboratory beams or numerical analysis; hence, the applicability of random forest to full-scale structures should be appraised. In this paper, the behavior of a constructed truss

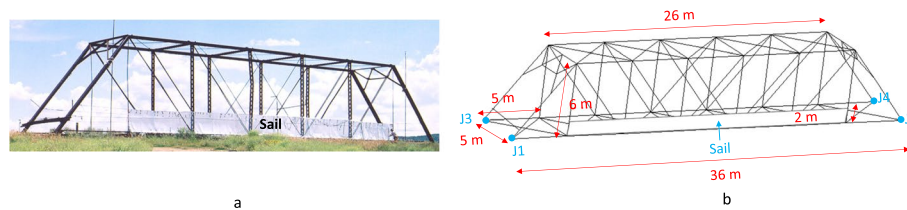


Fig. 1 The Four Mile Bridge in Steamboat Springs, Colorado: **a** site; **b** dimensions

bridge subjected to wind loadings is investigated through multidirectional approaches that consist of a field test, finite element modeling, and random forest.

2 Experimental program

2.1 Field testing

Information on field testing is excerpted from a previously conducted experimental program and further details are available elsewhere (Rutz 2004). A steel truss bridge, the Four Mile Bridge in Steamboat Springs, Colorado, USA, was instrumented and its responses were recorded under wind load (Fig. 1(a)). The 102-year-old bridge system, 36 m in length, 5 m in width, and 6 m in height, was composed of steel channels, eye bars, and hot-rolled cables for the chords and lateral bracings, as depicted in Fig. 1(b). Each chord was constituted with two eye bars possessing an elastic modulus of 200 GPa. The elastic modulus, yield strength, and ultimate strength of the cables were 159 GPa, 248 MPa, and 400 MPa, respectively. To properly measure wind loading, a plastic sail (26 m long by 1.6 m high) was placed on a windward side (Fig. 1(a)). Anemometers were positioned at five locations to log variable wind speeds (Fig. 2(a)): the individual locations were designated as WS1 to WS5. In addition, eight strain transducers were installed to the truss members for the quantification of wind-induced responses (Fig. 2(b)), which were recorded at every 0.1 seconds.

2.2 Wind-induced force

The dynamic pressure of wind (p) is expressed as.

$$p = \frac{1}{2} \rho v^2 \quad (1)$$

where ρ is the fluid mass density ($\rho = 1.225 \text{ kg/m}^3$ for sea-level air at 15°C , Carta and Mentado 2007) and v is the wind velocity in m/s. As far as a truss system is concerned, the pressure in Pascals may be attained from (Fouad and Calvert 2003).

$$p = 0.613 C_d v^2 \quad (2)$$

where C_d is the shape-dependent drag coefficient ($C_d = 2$ and 1.7 for the truss members and the sail, respectively, Hoerner 1958). As mentioned earlier, multiple strain transducers were employed to examine the response of the truss eye bars (Fig. 2(c)). Two bottom chords were selected at midspan and two eye bars A and B (Fig. 2(c)) were paired to form one chord (Fig. 2(b), where C1 and C2 are visible on the leeward and windward

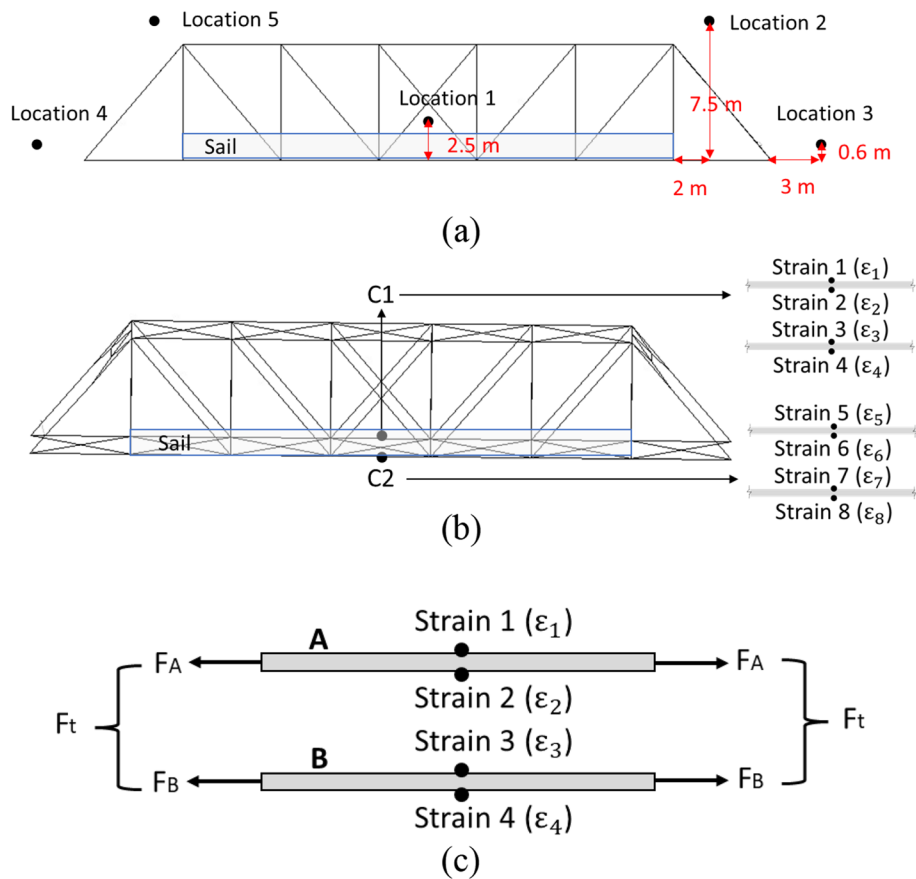


Fig. 2 Experimental setup: **a** locations for measuring wind speed; **b** monitored members; **c** calculation of wind-induced forces

sides, respectively). Using fundamental mechanics, the force of C1 (F_{t1}) was calculated by.

$$F_{t1} = F_A + F_B = EA(\varepsilon_A + \varepsilon_B) \tag{3}$$

where F_A and F_B are the forces of the eye bars A and B, respectively; E and A are the elastic modulus and the cross-sectional area of the bars, respectively ($E=200$ GPa and $A=1129$ mm²); and ε_A and ε_B are the axial strains of the A and B bars, respectively. Considering the strain reading scheme (ε_1 through ε_4) given in Fig. 2(c),

$$\varepsilon_A = \frac{(\varepsilon_1 + \varepsilon_2)}{2} \tag{4}$$

$$\varepsilon_B = \frac{(\varepsilon_3 + \varepsilon_4)}{2} \tag{5}$$

Substituting Eqs. 4 and 5 into Eq. 3 yields.

$$F_{t1} = EA \frac{(\varepsilon_1 + \varepsilon_2 + \varepsilon_3 + \varepsilon_4)}{2} \tag{6}$$

Similarly, the force of C2 (F_{t2}) can be determined. Shown in Figs.3 (a) and (b) are the measured wind speeds and the member strains, respectively.

2.3 Characterized wind speed

Because the magnitude of wind speed is not deterministic, a two-parameter Weibull distribution was adopted to characterize the speed. The probability density function ($f(v)$) and the cumulative distribution function ($F(v)$) of the Weibull distribution are written as (Bhattacharya and Bhattacharjee 2010; Ozay and Celiktas 2016).

$$f(v) = \frac{k}{c} \left(\frac{v}{c}\right)^{k-1} e^{-\left(\frac{v}{c}\right)^k} \tag{7}$$

$$F(v) = 1 - e^{-\left(\frac{v}{c}\right)^k} \tag{8}$$

where k and c are the shape and scale parameters, respectively. For the determination of these parameters, an open-source Python library called SciPy was used (Van Rossum and Drake 1995). The library is considered a comprehensive Python package specialized in solving multiple functions (Virtanen et al. 2020), which calculated the maximum likelihood of the wind speeds at a minimum difference between the recorded and calibrated values.

3 Modeling

3.1 Machine learning

3.1.1 Random forest

Random forest, a machine learning approach, was adopted to predict the wind-induced strains of the truss members. The tree-based decision-making algorithm is commonly known as Classification and Regression Trees (CART); therefore, both classification and regression problems can be solved without the configuration of structural members. A classification tree was used for the purpose of this research, which was implemented by the program R and associated libraries. A decision tree

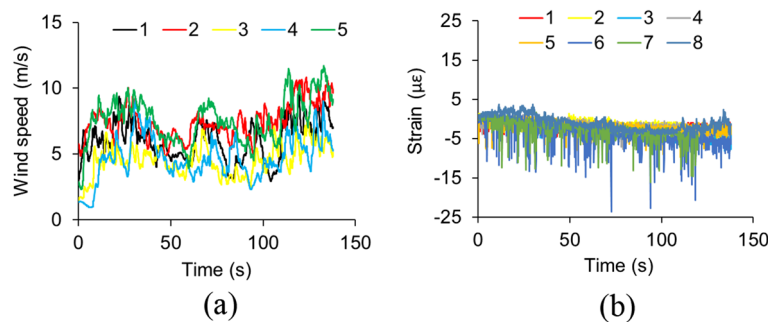


Fig. 3 Experimental results: **a** wind speeds; **b** wind-induced strains

model using classifiers is one of the most widely used predictive algorithms with popular features that include rapid classification, filtered trivial attributes, optimal efficiency, and affordable computational resources (Breiman 2017; Sheppard 2017). Figure 4 illustrates the procedural implementation of the random forest method. In accordance with a multilayered hidden training method that handled a total of 500 decision trees, randomly selected wind speeds were branched and corresponding member strains were linked. The experimentally obtained 1104 datasets were used to train the model (80% of the entire datasets) until convergence was achieved, which was then validated against the remaining 276 datasets.

3.1.2 Validation

Figure 5 demonstrates the measured and predicted strains of selected members. Most residual mean squares were less than 0.6; however, strain 6 of member C2 (Fig. 2(b)) revealed a relatively high value of 2.54, which could be attributed to either the uneven distribution of on-site wind or the local misalignment of the installed strain transducer.

3.2 Finite element analysis

A three-dimensional finite element model was developed using Rapid Interactive Structural Analysis for 3D Structures (RISA3D) to predict the behavior of the bridge under wind loading (Fig. 6). Frame elements represented individual truss members. Given that actual degrees of freedom at the supports of the historic bridge were unknown, a possible combination of various boundary conditions was taken into account (Table 1) at support locations J1 to J4 (Fig. 1(b)). When computing the axial forces of the C1 and C2 members (Fig. 2(b)), the applicability of two wind load models was assessed (Table 2).

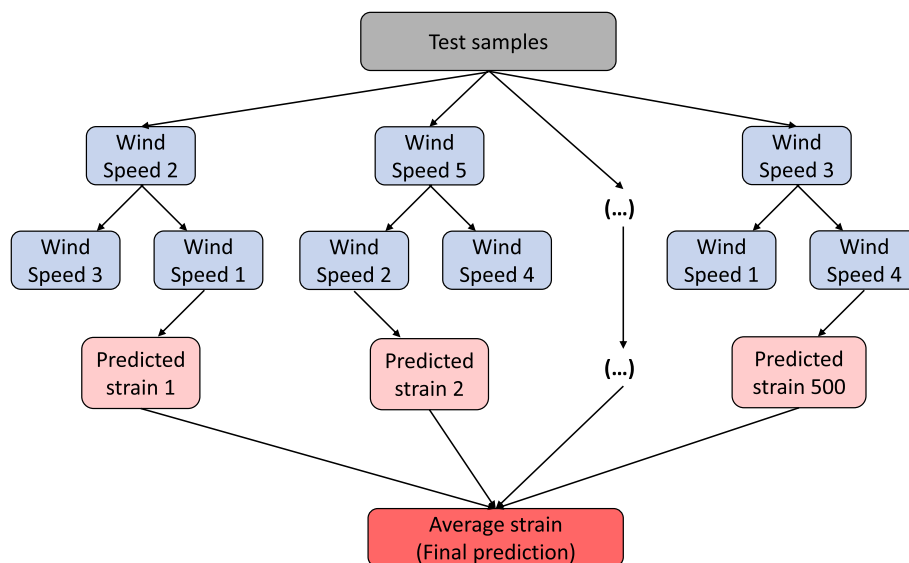


Fig. 4 Procedural implementation of random forest

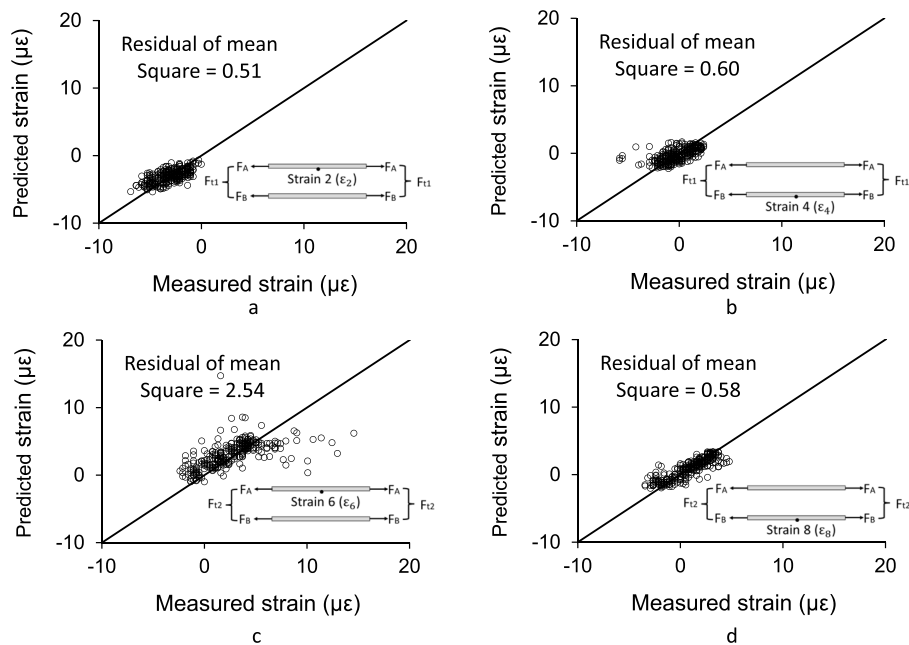


Fig. 5 Validation of random forest: **a** Strain 2; **b** Strain 4; **c** Strain 6; **d** Strain 8

3.2.1 Uniformly distributed wind pressure

The logged wind speeds at the five locations were converted to corresponding pressures by Eq. 2 and their average was applied to the truss model. Additionally, the wind loads appertaining to the sail pressures were equally divided into 12 points and applied to the truss members at the mid-heights of the members (Fig. 6(a)).

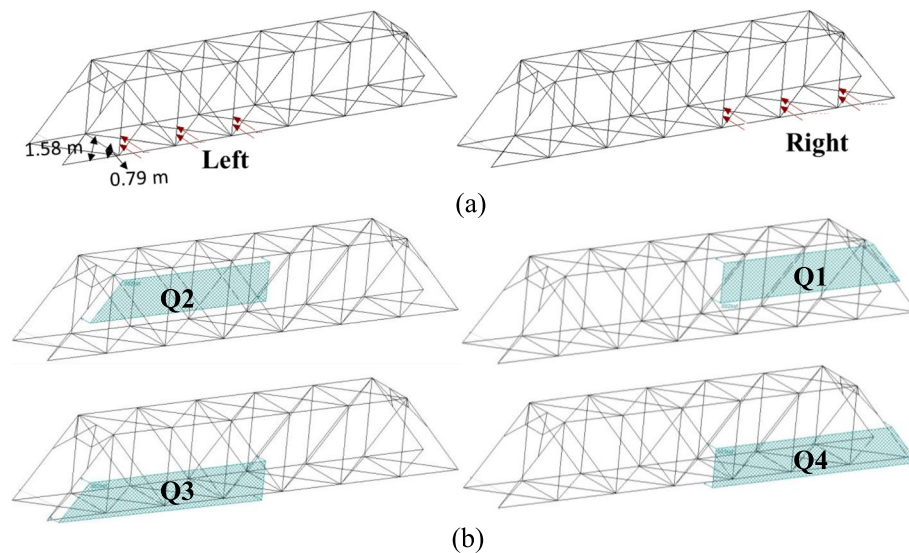


Fig. 6 Finite element model: **a** point load; **b** pressure load in a quadrant

Table 1 Boundary conditions of the historic truss bridge

Symbol	Support location	
	J1 and J3	J2 and J4
B1	Fixed	Fixed
B2	Fixed	Pinned
B3	Pinned	Fixed
B4	Fixed	Roller
B5	Roller	Fixed
B6	Pinned	Pinned
B7	Pinned	Roller
B8	Roller	Pinned

Table 2 Distribution of wind loads

Location	Uniform distribution				Quadrantal distribution			
	v (m/s)	p (Pa)	Average p (Pa)	Point load (kN)	v (m/s)	p (Pa)	Average p (Pa)	Point load (kN)
1	6.04	34.88	36.76	0.11	NA	NA	NA	NA
2 (Q1)	7.43	52.89			6.74	43.32	NA	0.10
3 (Q4)	4.54	19.72			5.29	26.71		
4 (Q3)	4.72	21.31			5.38	27.62	NA	0.10
5 (Q2)	7.58	54.98			6.81	44.27		

v = wind velocity; p = dynamic pressure of wind; Q1 to Q4 = pressures in a quadrant

Table 3 Parameters of Weibull distribution for wind speed

Weibull parameter	WS1	WS2	WS3	WS4	WS5
k	4.62	5.84	4.32	3.13	4.91
c	6.61	8.00	4.99	5.26	8.26

WS1 to 5 = location of wind speed measurement

3.2.2 Quadrantally distributed wind pressure

An integrated loading scheme was considered in a quadrant, as depicted in Fig. 6(b). The mean wind speed taken from Locations 1 to 5 (Fig. 2(a)) was applied to the simplified regions of Q1 to Q4 (Fig. 6(b)). Analogous to the uniform wind loading case, 12 point loads were applied to the members where the sail was positioned.

4 Results

4.1 Wind speed

According to the calibrated Weibull parameters (Table 3), the probability density functions at the five locations where the wind speeds were collected are plotted in Figs. 7(a) to (e). Although not shown in Fig. 7, considerable linearity was noticed between the ordered wind data and the quantiles of the Weibull distribution, confirming the adequacy of generating the probability curves. When the height of the sampling location elevated, the magnitude of the wind speed increased. For example, the mean speed

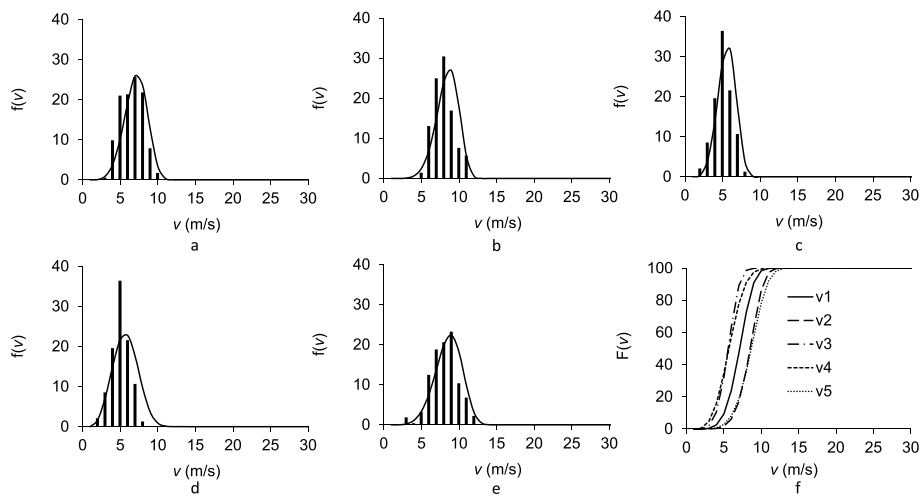


Fig. 7 Weibull distribution of wind speed: **a** Location 1; **b** Location 2; **c** Location 3; **d** Location 4; **e** Location 5; **f** comparison

Table 4 Probability of occurrence

Probability (%)	Wind speed (m/s)				
	WS1	WS2	WS3	WS4	WS5
20	4.78	6.21	3.53	3.26	6.08
40	5.72	7.15	4.29	4.25	7.20
60	6.48	7.87	4.87	5.10	8.09
80	7.33	8.67	5.59	6.12	9.12
99	9.16	10.28	6.97	8.49	11.18

WS1 to 5 = location of wind speed measurement

at Locations 2 and 5 was 7.5m/s, whereas the speed at Locations 3 and 4 was 4.6m/s. The trend of these wind speed variations is in line with archetypal wind distributions for structural design (ASCE 2016). The cumulative distribution functions graphed in Fig. 7(f) reaffirm the height-dependent wind speeds and further indicate that the wind speed at Location 1 can represent the overall speeds; in other words, the distribution at Location 1 was positioned between those at Locations 3 and 4 (lower positions) and at Locations 2 and 5 (higher positions). Based on the characterized wind speed distributions, the speeds at the five locations were predicted to cover occurrence probabilities ranging from 20% to 99% (Table 4).

4.2 Effects of boundary conditions

Shown in Fig. 8 are the forces of Members C1 and C2 (F_{t1} and F_{t2} , respectively) when subjected to the several boundary conditions (Table 1). There were inappreciable differences between the finite element models that incorporated the uniform and quadrantal pressure distributions, meaning that both cases reasonably reproduced the in-situ wind effects. The boundary conditions of B1 to B3 and B6 revealed an average absolute error of 55.8% and 51.9% in comparison with the experimentally attained forces of F_{t1} and F_{t2} ,

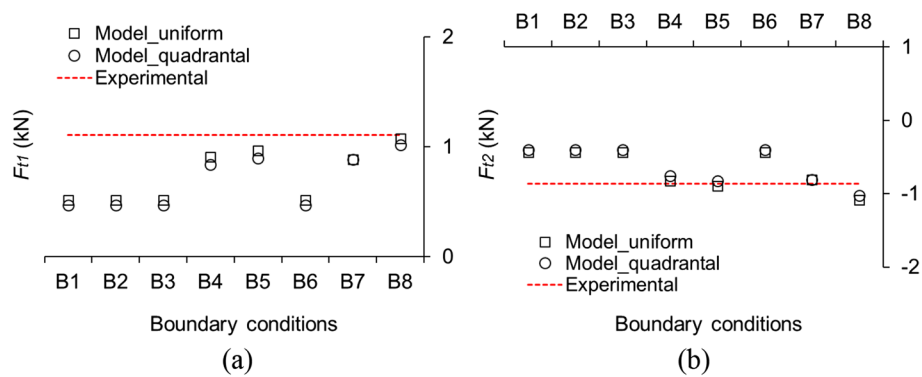


Fig. 8 Predicted member forces under various boundary conditions: **a** F_{t1} ; **b** F_{t2}

Table 5 Comparison of modeling approaches

Member	Axial load (kN)				Accuracy (%)		
	Exp.	FEM (uniform)	FEM (quadrantal)	Random forest	FEM (uniform)	FEM (quadrantal)	Random forest
C1	-0.86	-0.89	-0.83	-0.88	97	96	98
C2	1.11	0.97	0.9	0.9	87	76	82

respectively; on the contrary, the conditions of B4, B5, B7, and B8 provided the error of 15.8% and 10.0% for F_{t1} and F_{t2} , respectively. It is, thus, stated that partial fixities in the truss system were not significant and the conventional pin-roller connections at supports were found to be adequate. For this reason, the B5 condition with an average error of 9.9% for the F_{t1} and F_{t2} forces was taken for the model predictions discussed below.

4.3 Effects of pressure distributions

Table 5 compares the implications of the uniform and quadrantal pressure distributions for the member forces. Despite the marginal deviation of these distributions from the experimental values, the uniform distribution outperformed the quadrantal one at an average accuracy level of 92% and 86%, respectively. As such, the uniform distribution was selected for the present truss analysis.

4.4 Chord forces

The strain-based member forces of F_{t1} and F_{t2} are provided in Figs. 9(a) and (b), respectively. The scatter of these forces is ascribed to the stochastic nature of the wind. As in the case of characterizing the wind speeds, a normality test was carried out and their distribution was found to be Gaussian (Figs. 9(c) and (d)): the mean and standard deviation were -0.86 kN and 0.44 kN for F_{t1} and 1.11 kN and 0.75 kN for F_{t2} , respectively. Figures 10(a) and (b) display the F_{t1} and F_{t2} forces predicted by the random forest and finite element methods in conjunction with the predetermined occurrence probabilities of 20% to 99% (Table 6). These distinct approaches predicted close values; however, some discrepancies were noted possibly due to the fundamental uncertainties that took place in the field. Nonetheless, both of them were within a domain comprising the upper and lower limits of 95% and 5%, as visible in Figs. 10(c)

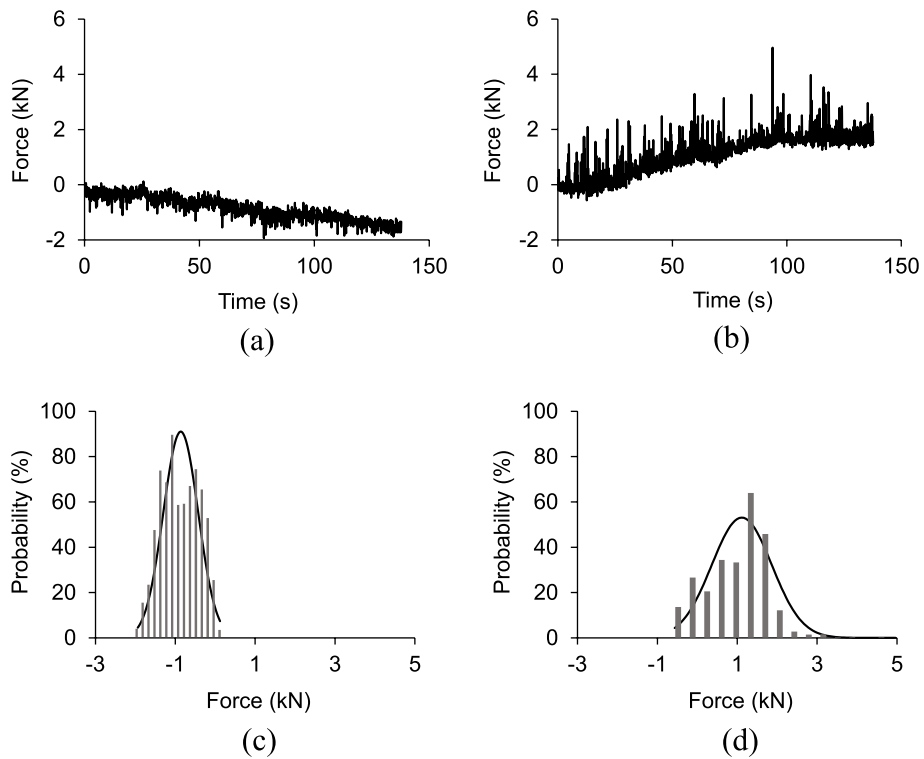


Fig. 9 Chord forces: **a** F_{t1i} ; **b** F_{t2i} ; **c** normal distribution of F_{t1i} ; **d** normal distribution of F_{t2i}

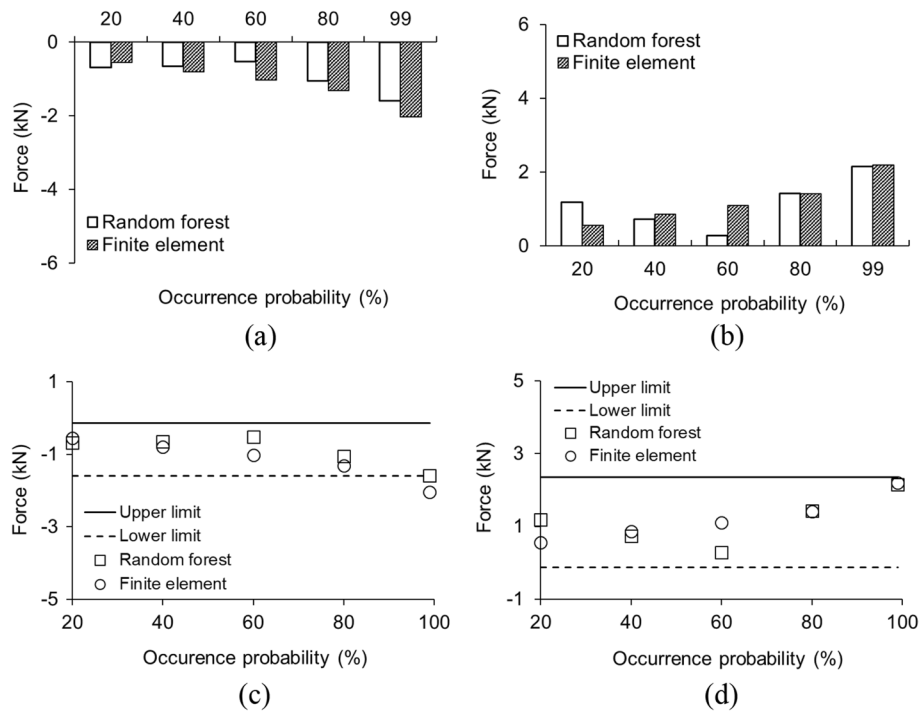


Fig. 10 Comparison of simulated forces: **a** F_{t1i} ; **b** F_{t2i} ; **c** limits for F_{t1i} ; **d** limits for F_{t2i}

Table 6 Distribution of wind loads

Probability (%)	Location	Uniform distribution			
		v (m/s)	p (Pa)	Average p (Pa)	Point load (kN)
20	1	4.78	21.89	23.27	0.07
	2	6.21	36.94		
	3	3.53	11.93		
	4	3.26	10.19		
	5	6.08	35.37		
40	1	5.72	31.33	32.94	0.10
	2	7.15	48.95		
	3	4.29	17.62		
	4	4.25	17.26		
	5	7.20	49.56		
60	1	6.48	40.20	41.93	0.12
	2	7.87	59.23		
	3	4.87	22.72		
	4	5.10	24.85		
	5	8.09	62.64		
80	1	7.33	51.43	53.75	0.16
	2	8.67	71.97		
	3	5.59	29.88		
	4	6.12	35.89		
	5	9.12	79.58		
99	1	9.16	80.36	83.32	0.24
	2	10.28	101.15		
	3	6.97	46.53		
	4	8.49	69.03		
	5	11.18	119.51		

v = wind velocity; p = dynamic pressure of wind

and (d), corroborating the acceptable performance of random forest in relation to the traditional finite element model.

4.5 System-level response

For the expansion of the element-level investigations to system-level evaluations, five members (M1 to M5) and supports (J1 to J4) were selected (Fig. 11(a)) and their responses were examined under the Weibull-based wind load. Figure 11(b) clarifies that the experimental stress based on the wind recorded in the field was positioned in between the occurrence probabilities of 40% and 60%, representing a typical service situation. Beyond this load range, the member stresses appreciably increased up to 26.6 MPa at the probability of 99%. Regarding the support displacement in the longitudinal direction (Fig. 11(c)), the pinned supports (J2 and J4) did not move; conversely, the supports on the other side demonstrated asymmetric displacements, leading to the fact that the internal distribution of the wind was irregular.

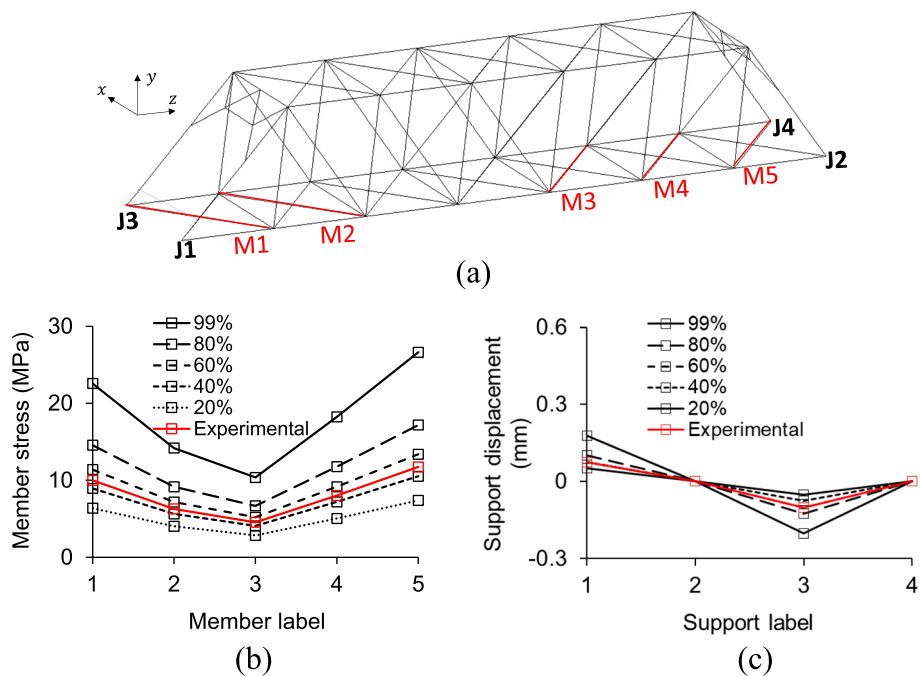


Fig. 11 Member response: **a** labeled joints and members; **b** member stress; **c** support displacement in the longitudinal direction

5 Summary and conclusions

This paper has discussed the behavior of a historic truss bridge subjected to wind load. Random forest, a machine learning approach, and three-dimensional finite element analysis were employed to examine the wind-induced responses of the 102-year-old bridge. The data measured in the field were utilized for the training and validation of the modeling approaches. A parametric study was performed to figure out the ramifications of several attributes such as pressure types (uniform and quadrantal), boundary conditions (fixities), and wind speeds (probabilistic inference). The predictability of the random forest and finite element models was comparable. The limitation of the current model is stated that it was built upon service wind loadings and did not include irregular circumstances (e.g., gusts). In future research, variable wind speeds may be employed to generate technical information that can evaluate design approaches related to extreme conditions. The following conclusions are drawn:

- The wind speeds collected from the site conformed to a Weibull distribution and were represented by its two-parameter model. The magnitude of the wind was a function of geospatial conditions; specifically, the wind intensity ascended with an increase in the elevation of the sampling location.
- The degree of partial fixities was not significant in the historic truss system; hence, the intended boundary conditions imposed when it was initially designed were maintained. Even if the uniform and quadrantal pressure distributions generated similar structural responses at the member level, the former better simulated the in-situ wind characteristics.

- Unlike the probability distribution of the wind speeds, the distribution of chord forces was Gaussian. The measured stress levels of the truss members were enveloped by those based on wind intensities between the occurrence probabilities of 40% and 60%. The irregular wind distributions resulted in the asymmetric behavior of the bridge supports.

Acknowledgements

The authors would like to acknowledge Dr. Frederick Rutz for providing wind data resource.

Authors' contributions

JW: Conceptualization, Methodology, Modeling, and Writing. JK: Conceptualization, Review, Editing, and Funding acquisition. LK: Modeling. All authors read and approved the final manuscript.

Funding

The authors are grateful for the support from the US Department of Transportation through the Mountain-Plains Consortium Program.

Availability of data and materials

The test data, FEM model, and machine learning model will be available upon reasonable request.

Declarations

Competing interests

The authors have no competing interests.

Received: 1 November 2022 Accepted: 10 November 2022

Published online: 22 November 2022

References

- AASHTO (2017) AASHTO LRFD bridge design specifications, 8th edn. American Association of State Highway and Transportation Officials, Washington, D.C.
- ANSI (1982) Minimum design loads for buildings and other structures. American National Standards Institute, Washington, D.C.
- ASCE (1990) Minimum design loads for buildings and other structures. American Society of Civil Engineers, Reston, VA
- ASCE (2010) Minimum design loads for buildings and other structures (ASCE 7–10). American Society of Civil Engineers, Reston, VA
- ASCE (2016) Minimum design loads and associated criteria for buildings and other structures (ASCE 7–16). Reston, VA
- Bhattacharya P, Bhattacharjee R (2010) A study on Weibull distribution for estimating the parameters. *Journal of Applied Quantitative Methods* 5(2):234–241
- Boulesteix A-L, Janitza S, Kruppa J, König IR (2012) Overview of random forest methodology and practical guidance with emphasis on computational biology and bioinformatics. *Data Min Knowl Disc* 2(6):493–507
- Breiman L (2017) Classification and regression trees. CRC Press, Boca Raton, FL
- Carta JA, Mentado D (2007) A continuous bivariate model for wind power density and wind turbine energy output estimations. *Energy Convers Manag* 48(2):420–432
- Chen W, Wang Q, Hesthaven JS, Zhang C (2021) Physics-informed machine learning for reduced-order modeling of nonlinear problems. *J Comput Phys* 446:110666
- Fawagreh K, Gaber MM, Elyan E (2014) Random forests: from early developments to recent advancements. *Sys Sci Control Eng* 2(1):602–609
- Fouad FH, Calvert E (2003) Wind load provisions in 2001 AASHTO supports specifications. *Transp Res Rec* 1845(1):10–18
- Han Y, Li K, He X, Chen S (2018) Stress analysis of a long-span steel-truss suspension bridge under combined action of random traffic and wind loads. *J Aerosp Eng* 31(3):04018021
- Hoerner SF (1958) Fluid-dynamic drag: practical information on aerodynamic drag and hydrodynamic resistance. Sonoran Nutra LLC, Phoenix, AZ
- Karpatne A, Kannan R, Kumar V (2023) Knowledge guided machine learning. CRC Press, Oxon, UK
- Li J, Hao H, Wang R, Li L (2021a) Development and application of random forest technique for element level structural damage quantification. *Struct Control Health Monit* 28(3):e2678
- Li L, Liang T, Ai S, Tang X (2021b) An improved random forest algorithm and its application to wind pressure prediction. *Int J Intell Syst* 36:4016–4032
- Lombardo FT (2021) History of the peak three-second gust. *J Wind Eng Ind Aerodyn* 208:104447
- Meher SK, Panda G (2021) Deep learning in astronomy: a tutorial perspective. *Eur Phys J Spec Top* 230:2285–2317
- Meshram V, Patil K, Meshram V, Hanchate D, Ramkteke SD (2021) Machine learning in agriculture domain: a state-of-art survey. *Artif Intell Life Sci* 1:100010
- Mohammed HRM, Ismail S (2021) Random forest versus support vector machine models' applicability for predicting beam shear strength. *Complexity* 2021:9978409

- Ozay C, Celiktas MS (2016) Statistical analysis of wind speed using two-parameter Weibull distribution in Alacati region. *Energy Convers Manag* 121:49–54
- Pham TA, Ly HB, Tran VQ, Giap LV, Vu HLT, Duong HAT (2020) Prediction of pile axial bearing capacity using artificial neural network and random forest. *Appl Sci* 10(5):1871
- Rutz FR (2004) Lateral load paths in historic truss bridges, PhD Dissertation, University of Colorado at Denver, Denver, CO
- Sheppard C (2017) Tree-based machine learning algorithms. CreateSpace Independent Publishing Platform, Scotts Valley, CA
- Sun T, Zhou Z-H (2018) Structural diversity for decision tree ensemble learning. *Front Comput Sci* 12:560–570
- Terranova N, Venkatakrishnan K, Benincosa LJ (2021) Application of machine learning in translational medicine: current status and future opportunities. *AAPS J* 23:74
- Thai H-T (2022) Machine learning for structural engineering: a state-of-the-art review. *Structures* 38:448–491
- Van Rossum G, Drake FL Jr (1995) Python tutorial. Centrum voor Wiskunde en Informatica, Amsterdam, The Netherlands
- Virtanen P, Gommers R, Oliphant TE, Haberland M, Reddy T, Cournapeau D, Burovski E, Peterson P, Weckesser W, Bright J, Van Der Walt SJ (2020) SciPy 1.0: fundamental algorithms for scientific computing in Python. *Nat Methods* 17(3):261–272
- Wassef W, Ragget J (2014) Updating the AASHTO LRFD wind load provisions, NCHRP project 20–07. Transportation Research Board, Washington, D.C.
- Wu T, Snaiki R (2022) Applications of machine learning to wind engineering. *Front Built Environ* 8:811460
- Zhang Y, Cardiff P, Keenahan J (2021) Wind-induced phenomena in long-span cable-supported bridges: a comparative review of wind tunnel tests and computational fluid dynamics modelling. *Appl Sci* 114(4):1642
- Zhu Z, Zhang Y (2021) Flood disaster risk assessment based on random forest algorithm. *Neural Comput & Applic* 34:3443–3455

Publisher's Note

Springer Nature remains neutral with regard to jurisdictional claims in published maps and institutional affiliations.

Submit your manuscript to a SpringerOpen[®] journal and benefit from:

- ▶ Convenient online submission
- ▶ Rigorous peer review
- ▶ Open access: articles freely available online
- ▶ High visibility within the field
- ▶ Retaining the copyright to your article

Submit your next manuscript at ▶ [springeropen.com](https://www.springeropen.com)
